https://doi.org/10.1016/j.actamat.2017.07.016

Shear and Shuffling Accomplishing Polymorphic fcc γ → hcp ε → bct α Martensitic Phase Transformation

Xu-Sheng Yang[b*], Sheng Sun[a*], Hai-Hui Ruan[c], San-Qiang Shi[c,d†], Tong-Yi Zhang[a‡]

[a]*Shanghai University Materials Genome Institute and Shanghai Materials Genome Institute, Shanghai University, 99 Shangda Road, Shanghai 200444, China*

[b]*Advanced Manufacturing Technology Research Centre, Department of Industrial and Systems Engineering, The Hong Kong Polytechnic University, Hung Hom, Kowloon, Hong Kong, China*

[c]*Department of Mechanical Engineering, The Hong Kong Polytechnic University, Hung Hom, Kowloon, Hong Kong, China*

[d]*Hong Kong Polytechnic University Shenzhen Research Institute, Shenzhen, China*

[*] These authors contributed equally to this work.

[†] Corresponding author. mmsqshi@polyu.edu.hk (S.-Q Shi). Tel & Fax: +852-27667821

[‡] Corresponding author. mezhangt@ust.hk and zhangty@shu.edu.cn (T.-Y Zhang). Tel & Fax: +86-21-66136172

Abstract

Martensitic transformation (MT) has extreme science merits and engineering significance. However, the underlying displacive atom collective movements for the transition from face-centered cubic structure (fcc-γ) austenites to body-centered tetragonal structure (bct-α) martensite has not been uncovered due to the lack of directly experimental evidence. Here, we examined the Plastic Deformation-Induced Martensitic Transformation (PDIMT) from fcc-γ to bct-α in AISI 304 stainless steel by High-resolution Transmission Electron Microscopy (HRTEM). The HRTEM observations exhibit a novel polymorphic fcc-γ → hcp-ε → bct-α PDIMT mechanism, which is further confirmed by the Molecular Dynamics (MD) simulations. The transition from fcc-γ to hcp-ε is accomplished by gliding Shockley partial dislocations on every second (111)γ planes. The transition from hcp-ε to bct-α is executed by gliding half-Shockley partial dislocation dipoles on every second (0001)ε planes and the gliding is simultaneously accompanied by atom shuffling. The dipole shear is conducted in a sandwich manner, meaning that a half-Shockley partial dislocation glides on one side of a (0001)ε plane and its partner of the dipole glides on the other side of the same (0001)ε plane. The novel findings will have great impact on the microstructural control in metals and alloys by PDIMT and stimulate innovative ideas to understand other solid phase transition mechanisms.

Keywords: Martensitic Transformation; bct Martensite; Stainless Steel; Shockley Partial Dislocation Dipole; High-Resolution Transmission Electron Microscopy

Introduction

Thermomechanical treatment of materials changes the material microstructure and therefore can improve the materials properties. The polymorphic change in solid crystalline structures is termed the solid-to-solid phase transformation. Martensitic Transformation (MT) describes a category of solid-to-solid displacive phase transition, where a collective movement of atoms occurs across distances that are typically smaller than one atomic nearest-neighbor spacing. Appropriate controlling MT is able to optimize the microstructure and improve the mechanical (e.g. strength, toughness, and shape memory [1-5]), electromagnetic (e.g. magneto- and mechano- and electro-caloric [6]), and transport (such as conductivity [7]) properties of materials. Both body-centered cubic (bcc) α' martensite and body-centered tetragonal (bct) α martensite can be transited from face-centered cubic (fcc) γ austenite via Plastic Deformation-Induced Martensitic Transformation (PDIMT). PDIMT may in turn cause TRansformation-Induced Plasticity (TRIP) effect, which has been observed in metastable austenitic steels, such as AISI 304 stainless steels [8, 9] and 301 stainless steels [10]. A martensitic particle has different volume and/or shape from its parent austenite of the same mass and composition as these of the martensitic particle. The change in volume and/or shape provides plasticity and strain-hardening, i.e., the TRIP effect. The transformed martensites effectively obstruct further plastic deformation locally and thus plastic deformation will continue in the relatively soft untransformed austenitic phase, thereby making the deformation more homogeneous and increasing the steel ductility. Obviously, it has extreme science merits and engineering significance to understand deeply the underlying microscopic mechanism of PDIMTs in steels, with sole crux lying in the collective movement of atoms.

MT in steels has been scientifically studied since the late 19th century [11, 12], and classic atomic shear models have been proposed to understand the collective movement of atoms during MT [13-15]. In 1964, Bogers and Burgers [15] proposed an ingenious hard-sphere shear model for a prototypical case of PDIMT from fcc-γ austenite phase to bcc-α′ martensite phase. Olson and Cohen [16-19] further developed the Bogers and Burgers model by emphasizing the role of plastic deformation, proposing that the fcc-γ phase transits to hexagonal close-packed hcp-ε martensite phase first and then to the bcc-α′ martensite phase. Yang *et al* [20, 21] called this model the Bogers-Burgers-Olson-Cohen model or the BBOC model for brevity. In the BBOC model, the shear component along $\langle 11\bar{2}\rangle\gamma$ direction on $\{111\}\gamma$ plane plays an essential role and this shear is conducted by the movement of Shockley partial dislocation with Burgers vector of $\frac{a_f}{6}\langle 11\bar{2}\rangle$ (a_f is the lattice constant of γ), especially in γ metals with low stacking fault energy. Gliding Shockley partial dislocations on every second $(111)\gamma$ planes cause the transition from fcc-γ to hcp-ε. The BBOC model describes the skeletal of the hcp-ε to bcc-α′ transition by gliding Shockley partial dislocations on two slipping systems. It is high resolution transmission electron microscopy (HRTEM) that provides the evidence of the collective movement of atoms at the atomic scale. The HRTEM images [20, 21] confirm the crucial role of partial dislocations, and reveal tell-tale features including the lattice rotation of the α′ martensite inclusion, the transition lattices at the ε/α′ interfaces that cater the shears, and the excess reverse shear-shuffling induced γ necks in the ε martensite laths. These direct observations at the atomic scale verify the 50-year-old BBOC model.

As mentioned above, fcc-γ phase may also be transited to body-centered tetragonal bct-α, such observed in gold and nickel [22-26]. Fig. S1 in Supplementary Information shows the

lattice correspondences for fcc-γ→ bcc-α' [12] and fcc-γ→ bct-α [22, 25, 26], respectively. The bcc-α′ with $a_{\alpha'} = b_{\alpha'} = c_{\alpha'}$ can be achieved by a 20% compression of the fcc-γ lattice in the $[001]\gamma$ direction, and an expansion of 12% in both $[110]\gamma$ and $[\bar{1}10]\gamma$ directions [12]. The bct structure with $a_\alpha = b_\alpha \neq c_\alpha$, however, is achieved by a 18.4% in the $[001]\gamma$ direction, a 15.3% expansion in the $[110]\gamma$ direction, and maintaining dimension unchanged in the$[\bar{1}10]\gamma$ direction [22, 25, 26]. Apparently, the bcc-α′ and bct-α martensites are two different phases with different lattice constants. However, the PDIMT from fcc-γ to bct-α martensite phase has not been systematically investigated yet, particularly, at the atomic level about the collective movement of atoms. The shear component gliding along $\langle 11\bar{2}\rangle\gamma$ direction on $\{111\}\gamma$ plane was reported to assist the nucleation of bct-α in the γ → α MT [23-25]. However, no evidence at the atomic level has reported so far about the polymorphic fcc-γ→ hcp-ε→ bct-α PDIMT. The present work provides such atomic level evidence by employing HRTEM observations on 304 stainless steel plastically deformed by the surface mechanical attrition treatment (SMAT). This success is attributed to the low stacking fault energy (~16.8 mJ/m^2) in 304 stainless steel [27] and the heterogeneous deformation field produced by SMAT, in which there is some region that provides the necessary transition condition for the polymorphic PDIMT from fcc-γ→ hcp-ε→ bct-α and thus the transition can be caught by careful examination of HRTEM.

The HRTEM observations on SMATed AISI 304 stainless steel with low stacking fault energy allow us to report a novel polymorphic γ → ε → α PDIMT based on Shockley partial dislocations and half Shockley partial dislocation dipoles. In addition, Molecular Dynamics (MD) simulations were carried out to confirm the HRTEM observed atomic arrangement at the γ/α interfaces. These evidences elucidate that the hcp-ε phase is also an intermediate phase in the

polymorphic PDIMT from fcc-γ to bct-α and the dipole slipping of half Shockley partial dislocations associated with atom shuffling completes the transition from the hcp-ε martensite to the bct-α martensite.

Experiments and MD simulations

The used 304 stainless steel had the composition of 0.04C, 0.49Si, 1.65Mn, 16.8Cr, 0.023P, 0.006S, 0.37Mo, 7.8Ni, and balance Fe in weight wt%. The sample for SMAT has the geometry of 70 mm × 50 mm × 1 mm. The SMAT technique was performed on two surfaces of the samples at room temperature for 15 mins with a vibrating frequency of 20 kHz and 3 mm bearing balls [28]. The plane-view TEM (JEOL 2010F) observations at different depth layers along the thickness direction were operated at voltage of 200 kV. The TEM samples were sliced from different depths of the SMATed samples to investigate the PDIMT evolution. The layered-TEM samples with thickness of ~20 μm were taken by mechanical polishing from different depths of the SMATed samples. Then the ion milling machine (Gatan Dual Ion Model 600) was used to prepare the TEM samples in the final stage.

The present atomistic simulations adopted the opening LAMMPS software [29] and the embedded-atom method (EAM) potential for Fe [30], which prefers the bcc structure in the temperature range of 0 to 1820 K. The reported lattice constant of fcc-γ in AISI 304 stainless steels [31, 32] ranges from ~3.56 Å to ~3.6 Å, due to the slightly change in the steel composition, and the lattice constant of hcp-ε can be calculated from the fcc-γ lattice constant. Direct measurements on HRTEM images [20, 21] give the lattice constants of fcc-γ and hcp-ε lattices in AISI 304 stainless steels to be 3.602 Å and 2.55 Å, respectively, and lattice constants of bct-α to be a = b =2.94 Å and c = 2.55 Å in the present measurement. If the present measured lattice

constants of bct-α are normalized by the measured fcc-γ lattice constant, the normalized lattice constants of bct-α are consistent with the reported values [22, 26]. These measured values of lattice constants are used in the atomistic simulations. The interface structures were built-up by following the experimentally observed orientation relationship, i.e., $[\bar{1}10]\gamma$ // $[11\bar{2}0]\varepsilon$ // $[00\bar{1}]\alpha$ and $(111)\gamma$ //$(0002)\varepsilon$ //$(110)\alpha$. In the atom setting, the nearest atomic distance was maintained larger than 2.0 Å inside the interface region to avoid the unreasonably severe local deformation. After that, the atoms in the interfacial region between -5 Å and 5 Å in the interface normal direction were allowed to relax at a given temperature to reach the minimum energy state, meanwhile the other atoms were fixed so that the entire simulation system could be maintained in multiply phases. In this way, the interface structure with minimum energy could be illustrated at the atomic level, especially, misfit dislocations, if any. The present atomistic simulations are called MD simulations here for simplification, while they are not exactly MD simulations because the MT was not simulated in the present work. The advantages of the present MD simulations lay in that the minimum energy interface structure between austenitic and martensitic phases could be visualized at the atomic level from different projection zones in three-dimensional space. The box size of the simulation system was 400 × 400 × 100 Å, with bct-α and fcc-γ (or hcp-ε) phases occupying the lower, [-50, 0] Å, and upper, [0, 50] Å, halves, respectively, along the *z* direction. The simulation box contained 1,436,611 and 1,404,575 atoms for bct/fcc and bct/hcp systems, respectively. Periodic boundary conditions were applied along the *x* and *y* directions. With the *NVT* ensemble (*N*, *V*, *T* denotes number of atoms, volume, and temperature, respectively) at temperature 2 K, energy minimization with conjugate gradient method was performed and followed by 1000 steps relaxation with the time step of 1 fs. The

software of OVITO [33] and the common neighbor analysis method [34] were employed to visualize and distinguish the atomic arrangements.

Results and Discussion

The polymorphic γ → ε and ε→ α PDIMTs were captured by HRTEM examination of the SMATed samples along its thickness direction. Figs. 1 (a-f) display the TEM images and associated selected area diffraction (SAD) patterns of the virginal un-SMATed samples (a) and SMATed samples at different depth (b-f), respectively, showing only few dislocations inside the un-SMATed samples (a), whereas high densities of dislocation grids in the centered layer (b), hcp-ε martensitic laths at ~ 90 μm depth layer (c), and bct-α martensite inclusions from one ε martensitic lath at the top layer of the SMATed samples (d-f). The experimental results suggest the consequence of deformation mechanism from dislocation activity to PDIMT fcc-γ → hcp-ε and then to PDIMT hcp-ε → bct α, as the plastic deformation gets more severe.

Figs. 2(a-c), respectively, give the HRTEM (a, b) and MD simulation (c) images at the γ/ε interfaces, viewed along $[\bar{1}10]\gamma$ // $[11\bar{2}0]\varepsilon$ directions, showing that the hcp-ε laths were generated via the glide of Shockley partial dislocations on every second $(111)\gamma$ planes. Noticeably, those partial dislocations may not all have the same Burges vectors, as indexed in Figs. 2(a-c). Fig. S2 in Supplementary Information indicates three types of Shockley partial dislocations, which have respectively Burges vectors of $\boldsymbol{b}_{\mathbf{p1}} = \frac{a_f}{6}[\bar{1}2\bar{1}](111)\gamma$, $\boldsymbol{b}_{\mathbf{p2}} = \frac{a_f}{6}[2\bar{1}\bar{1}](111)\gamma$, and $\boldsymbol{b}_{\mathbf{p3}} = \frac{a_f}{6}[\bar{1}\bar{1}2](111)\gamma$ on $(111)\gamma$ plane, where the dislocation line is along the $[\bar{1}10]\gamma$ direction. Gliding each of the three types of partials in fcc metals can create the same stacking fault, and cause deformation twins or detwinning, when gliding one partial on everyone

$(111)\gamma$ planes [35-37], and hcp-ε laths, when gliding one partial on every second $(111)\gamma$ planes [38]. However, the components of the three Burges vectors of $\boldsymbol{b}_{p1}$, $\boldsymbol{b}_{p2}$ and $\boldsymbol{b}_{p3}$ along the $[\bar{1}10]\gamma$ direction are different, which will lead to different shears along the $[\bar{1}10]\gamma$ direction when gliding the three types of partials. This might affect the intergranular misorientation [39], and thus the accomplishment of ε → α PDIMT is only executed by one type of partials of $\boldsymbol{b}_{p1}$, $\boldsymbol{b}_{p2}$ and $\boldsymbol{b}_{p3}$, which will be described below.

At the top surface layer of SMATed samples, there are α inclusions nucleated inside the ε laths, as evented by the HRTEM images and associated fast Fourier transformation (FFT) patterns in Figs. 3(a-e) and Figs. 1(d-f). Particularly, Fig. 3(a) shows that a ~10 nm bct-α inclusion is completely within a single ε lath, thereby suggesting that the bct-α matensite phase is transited from the ε martensite phase. Once nucleated, the α inclusion might grow and its width could be larger than the width of one single ε lath. For example, Figs. 1(d-f) presents a bigger α inclusion, ~70 nm in length and ~60 nm in width, surrounded by several parallel ε laths. The orientation relationship between the γ, ε and α, viewed along the $[\bar{1}10]\gamma$ // $[11\bar{2}0]\varepsilon$ // $[00\bar{1}]\alpha$ directions, are determined from the HRTEM images and associated FFT patterns, and schematically summarized in Fig. 3(f). The result shows that the closet packing planes $(111)\gamma$ preserves unrotated: $(111)\gamma$ //$(0002)\varepsilon$ //$(110)\alpha$ with the Kurdjumov-Sachs (K-S) orientation relationship [13]. In addition, the $(1\bar{1}0)\alpha$ planes are also parallel to the $(1\bar{1}00)\varepsilon$ planes.

Three noticeable characteristics in the γ → ε → α PDIMT are drawn from the FFT patterns in Figs. 3(b-f) and the HRTEM images in Figs. 3(g-h). The first characteristic is that the

inclined angle of $(11\bar{1})\gamma$ plane to $[11\bar{2}]\gamma$ direction is 70.52° in the parent fcc-γ phase, which transits to 90° of $(1\bar{1}0)\alpha$ plane to $[1\bar{1}0]\alpha$ direction in the final bct-α phase. The second is that the atomic spacing along the $[1\bar{1}0]\alpha$ direction ($d_{[1\bar{1}0]\alpha}$ = 2.08 Å) in the bct-α crystal is smaller than the corresponding one along the $[11\bar{2}]\gamma$ direction ($d_{[11\bar{2}]\gamma}$ = 2.21 Å) in the fcc-γ crystal, although the atomic planar spacing of $(11\bar{1})\gamma$ and $(1\bar{1}0)\alpha$ are equivalent, $d_{(11\bar{1})\gamma}$ = $d_{(1\bar{1}0)\alpha}$ = 2.08 Å. In other words, simultaneously increasing the inclined angle of $(11\bar{1})\gamma$ plane to $[11\bar{2}]\gamma$ direction and narrowing the atomic spacing along the $[11\bar{2}]\gamma$ direction cause the transition of bct-α from fcc-γ. The third characteristic is that the γ → ε transition process completes the half evolution of the inclined angle of $(11\bar{1})\gamma$ plane to $[11\bar{2}]\gamma$ direction, but keeps atomic spacing along the $[11\bar{2}]\gamma$ direction unchanged, as shown in Figs. 3(g-h).

To explore the atomic shear movement in the second-step ε → α transition, HRTEM and atomistic simulations are focused on the α/ε interface. Figs. 4(a-b) are respectively the HRTEM (a) and atomistic MD simulation (b) images in the α/ε interface regions, showing that the α/ε interface is diffuse between the $(1\bar{1}00)\varepsilon$ and $(1\bar{1}0)\alpha$ planes projected along $[11\bar{2}0]\varepsilon // [00\bar{1}]\alpha$ directions. The diffuse interface between the $(1\bar{1}00)\varepsilon$ and $(1\bar{1}0)\alpha$ planes has a thickness of about 4 nm, as shown by the HRTEM image in Fig. 4(a). The detailed Burgers circuit in Supplementary Fig. S3 demonstrates interestingly that an array of half Shockley partial dislocation dipoles, $\frac{1}{2}\boldsymbol{b}_{p3}$: $-\frac{1}{2}\boldsymbol{b}_{p3}$, with the Burgers vectors of opposite sign, and one partial, $\frac{1}{2}\boldsymbol{b}_{p3}$, of the dipole gliding on one side of a $(0001)\varepsilon$ plane, while the partner of $-\frac{1}{2}\boldsymbol{b}_{p3}$ gliding on the other side of the same $(0001)\varepsilon$ plane. The dipole slipping occurs on the every second $(0001)\varepsilon$

planes, thus changes the inclined angle of 70.52° between $(11\bar{1})\gamma$ plane and $[11\bar{2}]\gamma$ direction to 90° between $(1\bar{1}0)\alpha$ plane and $[1\bar{1}0]\alpha$ direction. As indicated in Fig. 4(a), slipping a half of partial dislocation leads to unstable stacking fault and generates high internal stress field if the atomic spacing along the $[11\bar{2}]\gamma$ direction or the $[1\bar{1}00]\varepsilon$ direction remains unchanged at 2.21 Å. To release the unstable stacking fault energy and associated strain energy, the atoms shuffle themselves and thus the atomic spacing along the $[1\bar{1}0]\alpha$ direction becomes 2.08 Å. Apparently, the dipole slipping of half Shockley partial dislocations and atom shuffling play a pivotal role in accomplishing the ε → α transition. Fig. 4(c) illustrates schematically the lattice evolution from original fcc-γ, to intermediate hcp-ε, and final bct-α lattice and dissects the functions of the Shockley partial dislocations and the half Shockley partial dislocations dipoles. With projection along the $[\bar{1}10]\gamma$ direction, if the yellow atoms are in $(\bar{1}10)\gamma$ plane, then the red ones would be out (below or above) $(\bar{1}10)\gamma$ plane in Fig. 4(c). Gliding any Shockley partial dislocation $\boldsymbol{b}_{\mathbf{p}}$ ($\boldsymbol{b}_{\mathbf{p1}}$, $\boldsymbol{b}_{\mathbf{p2}}$ or $\boldsymbol{b}_{\mathbf{p3}}$) on $(\bar{1}10)\gamma$ planes converts the stacking sequence as: A → B, B → C, C → A. However, gliding $\boldsymbol{b}_{\mathbf{p1}}$ or $\boldsymbol{b}_{\mathbf{p2}}$ switches the status of "in" and "out" $(\bar{1}10)\gamma$ plane atoms whereas gliding $\boldsymbol{b}_{\mathbf{p3}}$ does maintain the "in" status of $(\bar{1}10)\gamma$ plane atoms. This is because $\boldsymbol{b}_{\mathbf{p1}}$ and $\boldsymbol{b}_{\mathbf{p2}}$ have the shear components along the $[\bar{1}10]\gamma$ direction while $\boldsymbol{b}_{\mathbf{p3}}$ does not. As indicated in Fig. 4(c), when one type of the partial dislocations glides from plane B and successively on every second $(111)\gamma$ planes, the fcc-γ phase with stacking sequence of ⋯ABCABC⋯ will transit to the hcp-ε phase with stacking sequence of ⋯ACACAC⋯ and completes the half evolution of the inclined angle of $(11\bar{1})\gamma$ plane to $[11\bar{2}]\gamma$ direction, from 70.52° to 90°. The involved atoms in the transition from hcp-ε to bct-α should maintain the position "in" and "out" status of the $(\bar{1}10)\gamma$

plane atoms. Clearly, only this type of partial dislocations, $\boldsymbol{b}_{\mathbf{p3}}$, can meet the "in" and "out" requirement. Thus, dislocation dipole of $-\frac{1}{2}\boldsymbol{b}_{\mathbf{p3}}$ and $\frac{1}{2}\boldsymbol{b}_{\mathbf{p3}}$ gliding along the two sides of every second $(0001)\varepsilon$ planes in the "sandwich" manner switches the inclined angle from 70.52° of $(11\bar{1})\gamma$ to $[11\bar{2}]\gamma$ to 90° of $(1\bar{1}0)\alpha$ to $[1\bar{1}0]\alpha$. The dislocation dipole gliding is simultaneously accompanied by the atom shuffling that changes the atomic spacing. The array of Shockley partial dislocation dipoles were reported to change the stacking sequences in the low-energy, mobile grain boundaries in Magnesium [40], and phase transition in Laves phases $NbCr_2$ and $HfCr_2$ [41]. It is the first time in the present work to propose the role of half-partial dislocation dipoles in the phase transition from hcp-ε to bct-α in steels. Supplementary Fig. S4 gives the simulated image of the γ/α interfacial regions projected from the $[000\bar{1}]\varepsilon//[\bar{1}\,\bar{1}0]\alpha$, also showing the array of half Shockley partial dislocation dipoles, $-\frac{1}{2}\boldsymbol{b}_{\mathbf{p3}}$: $\frac{1}{2}\boldsymbol{b}_{\mathbf{p3}}$.

Because the collective movements of atoms are all activated on the $(111)\gamma$ / /$(0001)\varepsilon$ planes, the atomic planar spacing of the $(111)\gamma$ plane maintains unchanged in the whole evolution process, i.e., $d_{(111)\gamma} = d_{(0002)\varepsilon} = d_{(110)\alpha} = 2.08$ Å, as evented by the diffraction patterns in Fig. 3 and measured values of the intensity profiles that present the atomic planar spacing of $(111)\gamma$, $(0002)\varepsilon$ and $(110)\alpha$ planes in Supplementary Fig. S5(a-c). As mentioned above, atom shuffling reduces the atomic spacing $d_{[1\bar{1}\bar{2}]\gamma} = d_{[1\bar{1}00]\varepsilon} = 2.21$ Å along the $[11\bar{2}]\gamma$ and $[1\bar{1}00]\varepsilon$ directions to $d_{[1\bar{1}0]\alpha} = 2.08$ Å along the $[1\bar{1}0]\alpha$. Supplementary Fig. S5(d-f) and Fig. 5 show the experimental measurement result of atomic spacing at several representative atomic positions along the $[1\bar{1}00]\varepsilon$ direction from ε to α in the ε/α interface region of Fig. 4a, indicating that the gradually reduction of atomic spacing is completed by atom shuffling. The atom shuffling results

in the diffuse γ/α interface, which reduces the strain energy. Nevertheless, it is the atom shuffling that builds the bct-α atomic spacings $d_{(1\bar{1}0)\alpha} = d_{(110)\alpha}$ = 2.08 Å.

Fig. 6(a) depicts the Bain correspondence between the original fcc-γ and the final bct-α lattice (blue atoms) for the polymorphic γ → ε → α. The lattice constants of the bct-α lattice before deformation are expressed by $a_\alpha = c_\alpha = a_\gamma / \sqrt{2}$ = 2.55 Å and $b_\alpha = a_\gamma$ = 3.602 Å. The concurrent dislocation dipole gliding on every second $(0001)\varepsilon$ planes and atom shuffling lead to an increase of the inclined angle of $(11\bar{1})\gamma$ plane to $[11\bar{2}]\gamma$ direction, a compression along $[001]\gamma$ direction and an expansion along $[110]\gamma$ direction, as schematically indicated in Fig. 6(b), thereby giving $a_\alpha = b_\alpha = \sqrt{2}a_\gamma / \sqrt{3}$ = 2.94 Å in the transited bct-α lattice. After the reduction of atomic spacing along the $[11\bar{2}]\gamma // [1\bar{1}00]\varepsilon$ directions, the lattice misfit strain f = 5.88% is generated between $d_{[11\bar{2}]\gamma}$ = 2.21 Å and $d_{[1\bar{1}0]\alpha}$ = 2.08 Å. The spacing, l_d, of the misfit dislocation array $\boldsymbol{b} = \frac{a_f}{2}[\bar{1}01]$ on $(111)\gamma$ planes with γ as reference is determined by $l_d = b_{[11\bar{2}]\gamma} / f$ to be 37.57 Å, which is equivalent to the length of 18 $[1\bar{1}0]\alpha$ or 17 $[11\bar{2}]\gamma$ atomic spacings. As expected, the misfit dislocations are observed by MD simulations and HRTEM, as indicated in Figs. 6(c-d). When the α/γ interface with $(111)\gamma // (110)\alpha$ planes are viewed from $[\bar{1}\,\bar{1}\,2]\gamma // [\bar{1}10]\alpha$ directions, the interface is perfectly coherent with $c_\alpha = a_\gamma / \sqrt{2}$ = 2.55 Å, as shown by the MD simulation image in Fig. 6(f). Supplementary Fig. S6(a-c) illustrates schematically the evolution of atomic arrangements from γ lattice to ε and final α lattices with different projection views, elucidating the role of Shockley partial dislocations and atom shuffling along the $[11\bar{2}]\gamma // [1\bar{1}00]\varepsilon$ directions. Besides the HRTEM view, Supplementary Fig.

S6(b) shows the lattice evolution projected along the $[11\bar{2}]\gamma // [1\bar{1}00]\varepsilon // [\bar{1}10]\alpha$ directions, which is rotated 90 degrees from the HRTEM view and also indicates the value of $c_\alpha = a_\varepsilon = a_\gamma / \sqrt{2}$ = 2.55 Å keeps unchanged in the whole polymorphic MT process. Supplementary Fig. S6(c) is the lattice evolution projected along the $[101]\gamma // [\bar{1}2\bar{1}0]\varepsilon$ directions (rotated 60 degrees from the HRTEM view), corresponding to the $[\bar{1}1\bar{1}]\alpha$ direction in the final bct-α lattice but unparalleled. The relationship in lattice constants between the transited α and the original γ lattices in the present work agrees with that of surface-stress-induced γ →α transition in gold nanowires [22, 26].

Figs. 7(a-c) schematically compare the atomic shear mechanism of the γ → ε → α PDIMT in the present work to that of the γ → ε → α′ PDIMT [20, 21]. In the γ → ε → α′ PDIMT, an ε lath is formed by gliding "*T/2*" shear on every one of $\{111\}\gamma$ planes, if considering one Shockley partial dislocation as one "*T*". The transition of γ → ε → α′ is executed by two simultaneous shears of "*T/3*" ($\frac{a_f}{18}[1\bar{2}\bar{1}]$ on each $(11\bar{1})\gamma$ plane) and "*3T/8*" ($\frac{a_f}{16}[\bar{1}2\bar{1}]$ on each $(111)\gamma$ plane) [20, 21]. The "*T/3*" and "*3T/8*" shears are both modulated and spread from the "*T/2*" shear, thereby causing excess "*T/6*" and "*T/8*" shears, respectively, that must shear reversely to the γ phase. This mechanism works for the α′ phase nucleated at the intersection of two ε laths and within one single ε laths, as shown in Figs. 7(a-b). Obviously, the atomic movement mechanism of fcc-γ → hcp-ε → bct-α PDIMT observed in the present work is completely different from that of γ → ε → α′ reported before [20, 21]. Firstly, as shown in Fig. 7(c), the bct-α inclusion nucleates only from one single ε laths, with all atomic shear movements purely on $(111)\gamma // (1000)\varepsilon$ planes, whereas two shears on two planes ($(11\bar{1})\gamma$ and $(111)\gamma$) occur in the γ

→ ε → α′ PDIMT. Secondly, the sandwich manner gliding of the half Shockley partial dislocation dipoles of $-\frac{1}{2}\mathbf{b_{p3}}$ **:** $\frac{1}{2}\mathbf{b_{p3}}$ on every second $(0001)\varepsilon$ planes and atom shuffling of narrowing the atomic spacing along the $[1\bar{1}00]\varepsilon$ / /$[11\bar{2}]\gamma$ directions accomplish the transition from hcp-ε to bct-α. Although the Shockley partial dislocation dipole movement mechanism was reported in the change of the stacking sequence in the low-energy, mobile grain boundaries [40], it is the first time in the present work to propose the role of half-partial dislocation dipoles in the phase transition, from hcp-ε to bct-α in steels.

Concluding Remarks

In summary, heterogeneous plastic deformation of 304 stainless steel and watchful HRTEM examinations make it possible to dissect the polymorphic γ → ε → α PDIMT with bct-α nucleated from hcp-ε laths. Based on the HRTEM observations, a novel PDIMT mechanism from hcp-ε to bct-α is proposed with simultaneous gliding of half-Shockley partial dislocation dipoles on every second $(0001)\varepsilon$ planes and atom shuffling. MD simulations confirm the HRTEM observations and the proposed model. This novel model predicts the atomic arrangements and crystalline defects at the interfacial regions between any two of the three γ, ε, and α crystalline lattices. All the theoretical predictions agree with the HRTEM observations and MD simulations. There are three types of Shockley partial dislocations in fcc-γ lattice. Although gliding each of the three types of partial dislocations on every second $(111)\gamma$ planes transits fcc-γ to hcp-ε, only one type of Shockley partial dislocations, named $\boldsymbol{b}_{\mathbf{p3}}$ in the present work, functions in the transition from hcp-ε to bct-α. The sandwich manner gliding of half Shockley partial dislocation dipoles ($-\frac{1}{2}\boldsymbol{b}_{\mathbf{p3}}$: $\frac{1}{2}\boldsymbol{b}_{\mathbf{p3}}$) on every second $(0001)\varepsilon$ planes and atom shuffling of

narrowing the atomic spacing along the $[1\bar{1}00]\varepsilon // [11\bar{2}]\gamma$ directions accomplish the transition from hcp-ε to bct-α. These new findings will inspire academic research on polymorphic solid-solid phase transitions and engineering practice on how to further improve material properties by utilize and control the phase transitions.

References:

[1] K. Otsuka, T. Kakeshita, Science and technology of shape-memory alloys. New developments, MRS Bull. 27 (2002) 91-100.

[2] M. Militzer, A Synchrotron Look at Steel, Science 298 (2002) 975-976.

[3] V.F. Zackay, E.R. Parker, D. Fahr, B. Bush, Enhancement of ductility in high-strength steels, Trans. Am. Soc. Metals 60 (1967) 252-259.

[4] K. Otsuka, C.M. Wayman, Shape memory materials, Cambridge University Press1999.

[5] Y. Song, X. Chen, V. Dabade, T.W. Shield, R.D. James, Enhanced reversibility and unusual microstructure of a phase-transforming material, Nature 502 (2013) 85-88.

[6] X. Moya, S. Kar-Narayan, N.D. Mathur, Caloric materials near ferroic phase transitions, Nat. Mater. 13 (2014) 439-450.

[7] B. Kalisky, E.M. Spanton, H. Noad, J.R. Kirtley, K.C. Nowack, C. Bell, H.K. Sato, M. Hosoda, Y. Xie, Y. Hikita, C. Woltmann, G. Pfanzelt, R. Jany, C. Richter, H.Y. Hwang, J. Mannhart, K.A. Moler, Locally enhanced conductivity due to the tetragonal domain structure in $LaAlO_3/SrTiO_3$ heterointerfaces, Nat. Mater. 12 (2013) 1091-1095.

[8] X.L. Wu, M.X. Yang, F.P. Yuan, L. Chen, Y.T. Zhu, Combining gradient structure and TRIP effect to produce austenite stainless steel with high strength and ductility, Acta Mater 112 (2016) 337-346.

[9] Y. Tomita, T. Iwamoto, Constitutive modeling of trip steel and its application to the improvement of mechanical properties, Int. J. Mech. Sci. 37 (1995) 1295-1305.

[10] J. Liu, Y. Jin, X. Fang, C. Chen, Q. Feng, X. Liu, Y. Chen, T. Suo, F. Zhao, T. Huang, H. Wang, X. Wang, Y. Fang, Y. Wei, L. Meng, J. Lu, W. Yang, Dislocation Strengthening without Ductility Trade-off in Metastable Austenitic Steels, Sci. Rep. 6 (2016) 35345.

[11] C.S. Smith, A History of Metallography: The Development of Ideas on the Structure of Metals Before 1890, The MIT. Press, Cambrige, Massachusetts London, England, 2012.

[12] E.C. Bain, N.Y. Dunkirk, The Nature of Martensite, Trans. Amer. Inst. Min. Metall. 70 (1924) 25.

[13] G. Kurdjumov, G. Sachs, über den Mechanismus der Stahlhrtung, Zeit. F. Phys 64 (1930) 325-343.

[14] Z. Nishiyama, X-Ray Investigation the Mechanism of Transformation from Face-Centred-Cubic Lattice to Body-Centred Cubic Sci. Rep. Tohoku Univ 23 (1934) 68.

[15] A.J. Bogers, W.G. Burgers, Partial dislocations on the {110} planes in the B.C.C. lattice and the transition of the F.C.C. into the B.C.C. lattice, Acta Metall. 12 (1964) 255-261.

[16] G.B. Olson, M. Cohen, A mechanism for the strain-induced nucleation of martensitic transformations, J. Less. Common Met. 28 (1972) 107-118.

[17] G.B. Olson, M. Cohen, A general mechanism of martensitic nucleation: Part II. FCC → BCC and other martensitic transformations, Metall. Mater. Trans. A 7 (1976) 1905-1914.

[18] G.B. Olson, M. Cohen, A Perspective on Martensitic Nucleation, Annu. Rev. Mater. Sci. 11 (1981) 1-30.

[19] G.B. Olson, M. Cohen, Dislocation Theory of Martensitic Transformations, in: F.R.N.Nabarro (Ed.) Dislocations in solids, North-Holland, Amsterdam. Oxford. New York. Tokyo, 1986.

[20] X.-S. Yang, S. Sun, X.-L. Wu, E. Ma, T.-Y. Zhang, Dissecting the Mechanism of Martensitic Transformation via Atomic-Scale Observations, Sci. Rep. 4 (2014) 6141.

[21] X.-S. Yang, S. Sun, T.-Y. Zhang, The mechanism of bcc α′ nucleation in single hcp ε laths in the fcc γ → hcp ε → bcc α′ martensitic phase transformation, Acta Mater. 95 (2015) 264-273.

[22] J. Diao, K. Gall, M.L. Dunn, Surface stress driven reorientation of gold nanowires, Phys. Rev. B 70 (2004) 075413.

[23] A. Nie, H. Wang, Deformation-mediated phase transformation in gold nano-junction, Mater. Lett. 65 (2011) 3380-3383.

[24] L. Wang, P. Liu, P. Guan, M. Yang, J. Sun, Y. Cheng, A. Hirata, Z. Zhang, E. Ma, M. Chen, X. Han, In situ atomic-scale observation of continuous and reversible lattice deformation beyond the elastic limit, Nat. Commun. 4 (2013).

[25] H. Zheng, A. Cao, C.R. Weinberger, J.Y. Huang, K. Du, J. Wang, Y. Ma, Y. Xia, S.X. Mao, Discrete plasticity in sub-10-nm-sized gold crystals, Nat. Commun. 1 (2010) 144.

[26] J. Diao, K. Gall, M.L. Dunn, Surface-stress-induced phase transformation in metal nanowires, Nat. Mater. 2 (2003) 656-660.

[27] H.W. Zhang, Z.K. Hei, G. Liu, J. Lu, K. Lu, Formation of nanostructured surface layer on AISI 304 stainless steel by means of surface mechanical attrition treatment, Acta Mater. 51 (2003) 1871-1881.

[28] A.Y. Chen, H.H. Ruan, J. Wang, H.L. Chan, Q. Wang, Q. Li, J. Lu, The influence of strain rate on the microstructure transition of 304 stainless steel, Acta Mater. 59 (2011) 3697-3709.

[29] S. Plimpton, Fast Parallel Algorithms for Short-Range Molecular Dynamics, J. Compu. Phys. 117 (1995) 1-19.

[30] M.I. Mendelev, S. Han, D.J. Srolovitz, G.J. Ackland, D.Y. Sun, M. Asta, Development of new interatomic potentials appropriate for crystalline and liquid iron, Philos. Mag. 83 (2003) 3977-3994.

[31] F.C. Nascimento, C.E. Foerster, S.L.R.d. Silva, C.M. Lepienski, C.J.d.M. Siqueira, C. Alves Junior, A comparative study of mechanical and tribological properties of AISI-304 and AISI-316 submitted to glow discharge nitriding, Mater. Res. 12 (2009) 173-180.

[32] P. Mangonon, G. Thomas, The martensite phases in 304 stainless steel, Metall. Mater. Trans. B 1 (1970) 1577-1586.

[33] A. Stukowski, Visualization and analysis of atomistic simulation data with OVITO–the Open Visualization Tool, Model. Simul. Mater. Sci. Eng. 18 (2010) 015012.

[34] J.D. Honeycutt, H.C. Andersen, Molecular dynamics study of melting and freezing of small Lennard-Jones clusters, J. Phys. Chem. 91 (1987) 4950-4963.

[35] X.L. Wu, Y.T. Zhu, Inverse Grain-Size Effect on Twinning in Nanocrystalline Ni, Phys. Rev. Lett. 101 (2008) 025503.

[36] J. Wang, N. Li, O. Anderoglu, X. Zhang, A. Misra, J.Y. Huang, J.P. Hirth, Detwinning mechanisms for growth twins in face-centered cubic metals, Acta Mater. 58 (2010) 2262-2270.

[37] B.Q. Li, M.L. Sui, B. Li, E. Ma, S.X. Mao, Reversible Twinning in Pure Aluminum, Phys. Rev. Lett. 102 (2009) 205504.

[38] H. Heinrich, H.P. Karnthaler, T. Waitz, G. Kostorz, Transformation dislocations in Co-Fe, Mater. Sci. Eng. A 272 (1999) 238-243.

[39] G. Lucadamo, D.L. Medlin, Geometric Origin of Hexagonal Close Packing at a Grain Boundary in Gold, Science 300 (2003) 1272-1275.

[40] X. Liu, J. Wang, Low-energy, Mobile Grain Boundaries in Magnesium, Sci. Rep. 6 (2016) 21393.

[41] J. Aufrecht, A. Leineweber, V. Duppel, E.J. Mittemeijer, Transformation–dislocation dipoles in Laves phases: A high-resolution transmission electron microscopy analysis, J. Mater. Res. 25 (2010) 1983-1991.

Acknowledgements

The present research is supported by the PolyU Post-Dr Research Grant (No. 1-YW1M) and the PolyU Start-up Fund for New Recruits (No. 1-ZE8R) from The Hong Kong Polytechnic University, NSFC (No. 51271157), and the research grants (No. 15DZ2260300 and No. 16DZ2260600) from the Science and Technology Commission of Shanghai Municipality.

Competing financial interests

The authors declare no competing financial interests.

Figure Captions

Figure 1. The polymorphic γ (fcc) → ε (hcp) → α (bct) martensitic transformation. (**a**) TEM image and associated selected area diffraction (SAD) patterns of the virginal un-SMATed samples. (**b-f**) TEM image and associated diffraction patterns at different depth from center depth (**b**), to layer ~90 μm from surface (**c**), and to the top surface layer (**d-f**) of the SMATed sample, respectively, showing the dislocation grids on the $\{111\}\gamma$ crystallographic planes (**b**), to the formation of the hcp-ε laths (**c**), and finally the bct-α martensitic inclusions nucleated along single ε laths (**d-f**).

Figure 2. γ → ε transformation. (**a-b**) HRTEM and (**c**) MD simulation images, projected along $[\bar{1}10]\gamma$ / /$[11\bar{2}0]\varepsilon$ directions, show that the hcp-ε martensitic laths can be generated via gliding each of three types of Shockley partial dislocations on every second $(111)\gamma$ planes. The three types of dislocations have Burgers vectors, $\boldsymbol{b}_{\mathbf{p1}} = \frac{a_f}{6}[\bar{1}2\bar{1}](111)\gamma$, $\boldsymbol{b}_{\mathbf{p2}} = \frac{a_f}{6}[2\bar{1}\bar{1}](111)\gamma$ and $\boldsymbol{b}_{\mathbf{p3}} = \frac{a_f}{6}[\bar{1}\bar{1}2](111)\gamma$, respectively, with respect to the $[\bar{1}10]\gamma$ tilt axis.

Figure 3. The ε → α transformation. (**a-e**) A bct-α martensitic inclusion within a single ε lath and the associated live diffraction spots for each phase. (**f**) Schematic summarizing the diffraction spots from (**b-e**) for the orientation relationships between the γ, ε and α, viewed along $[\bar{1}10]\gamma$ / /$[11\bar{2}0]\varepsilon$ / /$[00\bar{1}]\alpha$ directions, showing $(111)\gamma$ //$(0002)\varepsilon$ //$(110)\alpha$ with the Kurdjumov-Sachs (K-S) orientation relationship. (**g-h**) The atomic images, viewed along $[\bar{1}10]\gamma$ / /$[11\bar{2}0]\varepsilon$ / /$[00\bar{1}]\alpha$ directions, imply that the essential actions in the transition of α from γ, which are realized by simultaneously increasing the inclined angle of $(11\bar{1})\gamma$ plane to $[11\bar{2}]\gamma$ direction and narrowing the atomic spacing along the $[11\bar{2}]\gamma$ direction.

Figure 4. The α/ε interface. Projected along $[11\bar{2}0]\varepsilon$ / /$[00\bar{1}]\alpha$ directions, HRTEM (**a**) and atomistic MD simulation (**b**) images of α/ε interface regions show that an array of half Shockley partial dislocation dipoles, $-\frac{1}{2}\boldsymbol{b}_{\mathbf{p3}}$: $\frac{1}{2}\boldsymbol{b}_{\mathbf{p3}}$, with Burgers vectors of opposite sign, were characterized on every second $(0001)\varepsilon$ planes. (**c**) Schematic diagrams for the role of partial dislocations in the lattice evolutions from γ, to ε and finally α lattice. Gliding each of the three types of Shockley partial dislocations ($\boldsymbol{b}_{\mathbf{p1}}$, $\boldsymbol{b}_{\mathbf{p2}}$ or $\boldsymbol{b}_{\mathbf{p3}}$) on every second $(111)\gamma$ planes induces the γ → ε transition. Slipping an array of half 90° Shockley partial dislocation dipoles, $-\frac{1}{2}\boldsymbol{b}_{\mathbf{p3}}$: $\frac{1}{2}\boldsymbol{b}_{\mathbf{p3}}$, on every second $(0001)\varepsilon$ planes and narrowing atomic spacing via atoms shuffling along the $[1\bar{1}00]\varepsilon$ / /$[11\bar{2}]\alpha$ directions finish the ε → α transition.

Figure 5. The measurement result of atomic spacing at several representative atomic positions along the $[1\bar{1}00]\varepsilon$ direction from ε to α in the ε/α diffuse interface region of Fig. 4a, indicating that the gradually reduction of atomic spacing is completed by atom shuffling.

Figure 6. Lattice mismatch and misfit dislocations between fcc-γ and bct-α. (**a**) The Bain correspondence between the original fcc-γ and the final bct-α lattice (blue atoms) for the polymorphic γ→ α. (**b**) Projected along $[\bar{1}10]\gamma // [00\bar{1}]\alpha$ directions, the concurrent increase of the inclined angle of $(11\bar{1})\gamma$ plane to $[11\bar{2}]\gamma$, and a compression along $[001]\gamma$ and an expansion along $[110]\gamma$ transits the γ lattice to the α lattice with $a_\alpha = b_\alpha = \sqrt{2}a_\gamma / \sqrt{3}$ = 2.94 Å and c_α=2.55 Å. The MD simulation (**c**) and HRTEM (**d**) images of the α/γ diffuse interface between the $(111)\gamma$ plane and $(110)\alpha$ plane, view along $[\bar{1}10]\gamma // [00\bar{1}]\alpha$ directions, showing the misfit dislocation with Burgers vector of $\frac{a_f}{2}[\bar{1}01]$ on $(111)\gamma$ planes are distributed every either 18 $[1\bar{1}0]\alpha$ or 17 $[11\bar{2}]\gamma$ atomic spacings to release the misfit lattice stain between the γ and α. (**e**) MD simulation images of the γ/α interface region viewed along $[\bar{1}\bar{1}2]\gamma // [\bar{1}10]\alpha$ directions indicate a coherent interface with $(111)\gamma // 110)\alpha$ planes and $c_\alpha = a_\gamma / \sqrt{2}$ = 2.55 Å.

Figure 7. The comparison of the atomic movement procedure for the polymorphic (**a, b**) fcc-γ → hcp-ε → bcc-α′ and (**c**) fcc-γ → hcp-ε → bct-α PDIMT. Especially, the sandwich manner gliding of one type of half Shockley partial dislocation dipoles, named $-\frac{1}{2}\boldsymbol{b}_{\mathbf{p3}}$ **:** $\frac{1}{2}\boldsymbol{b}_{\mathbf{p3}}$, on every second $(0001)\varepsilon$ planes and atom shuffling of narrowing the atomic spacing along the $[1\bar{1}00]\varepsilon // [11\bar{2}]\gamma$ directions accomplish the transition from hcp-ε to bct-α.

Figure 1

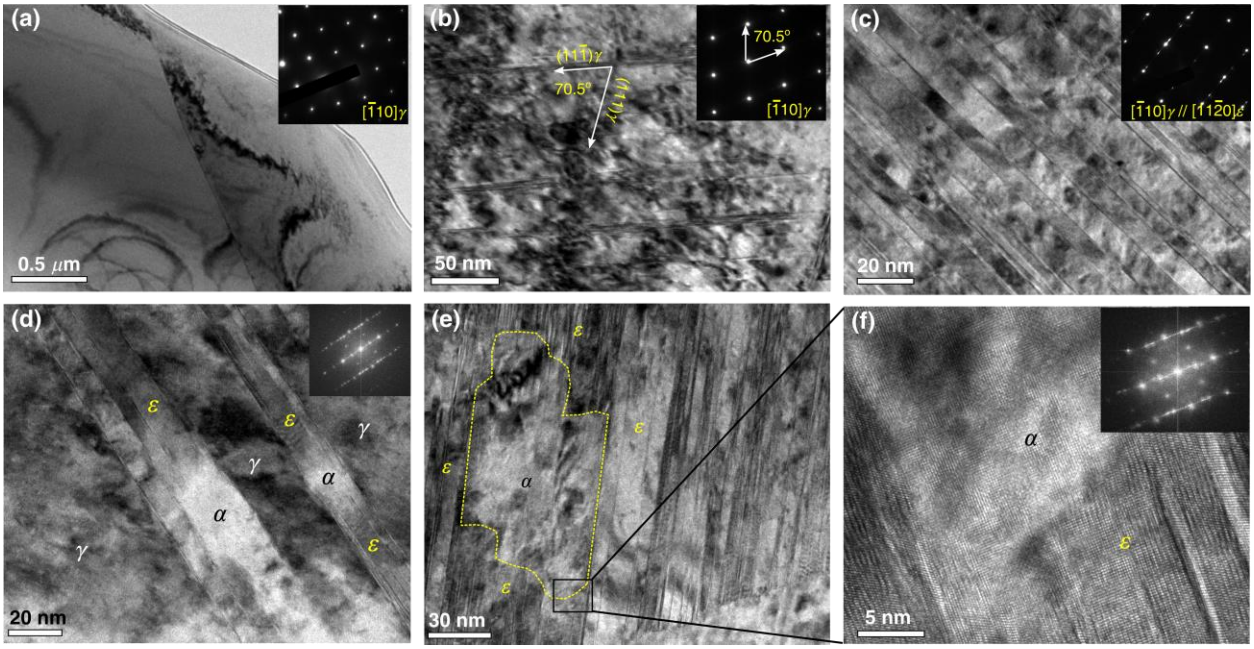
(a)
$[\bar{1}10]_\gamma$
0.5 μm
(b)
$(11\bar{1})_\gamma$
70.5°
$(\bar{1}11)_\gamma$
70.5°
$[\bar{1}10]_\gamma$
50 nm
(c)
$[\bar{1}10]_\gamma$ // $[\bar{1}1\bar{2}0]_\varepsilon$
20 nm
(d)
ε
ε
γ
γ
α
α
γ
ε
20 nm
(e)
ε
ε
α
ε
ε
30 nm
(f)
α
ε
5 nm

Figure 2

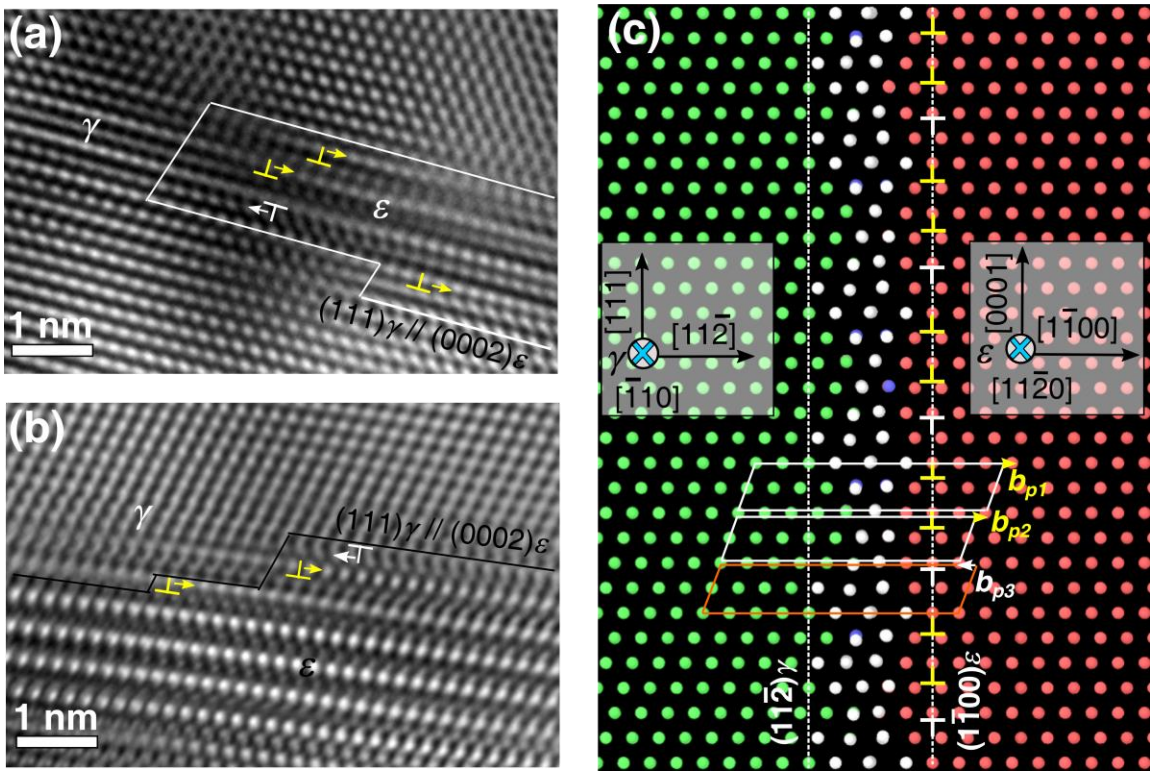
(a)
γ
ε
1 nm
(111)γ // (0002)ε
(b)
γ
(111)γ // (0002)ε
ε
1 nm
(c)
[111]
[11$\bar{2}$]
γ
[$\bar{1}$10]
[000$\bar{1}$]
[1$\bar{1}$00]
ε
[11$\bar{2}$0]
b_{p1}
b_{p2}
b_{p3}
(11$\bar{2}$)γ
(1$\bar{1}$00)ε

Figure 3

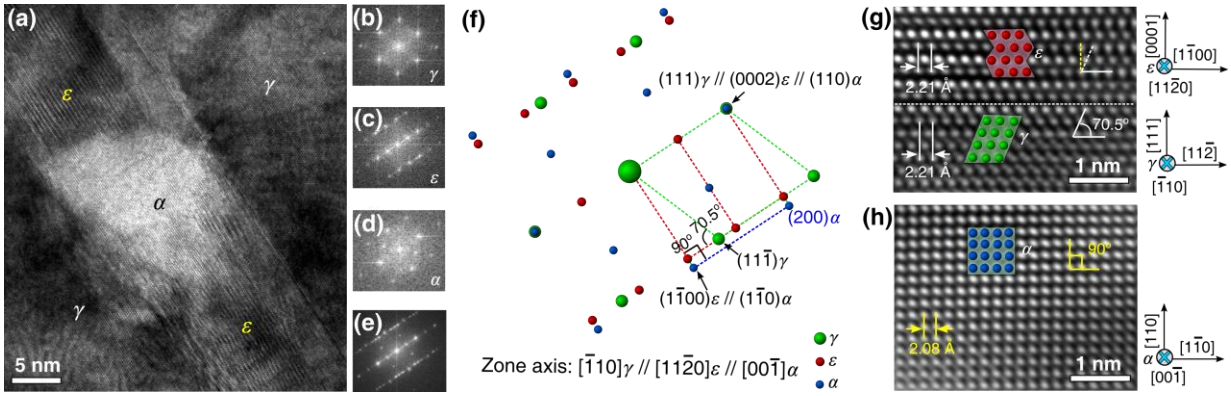
(a)
ε
γ
α
γ
ε
5 nm
(b)
γ
(c)
ε
(d)
α
(e)
(f)
(111)γ // (0002)ε // (110)α
(200)α
70.5°
90°
(11$\bar{1}$)γ
(1$\bar{1}$00)ε // (1$\bar{1}$0)α
Zone axis: [$\bar{1}$10]γ // [11$\bar{2}$0]ε // [00$\bar{1}$]α
γ
ε
α
(g)
2.21 Å
ε
2.21 Å
γ
70.5°
1 nm
[0001]
[1$\bar{1}$00]
[11$\bar{2}$0]
[111]
[11$\bar{2}$]
[$\bar{1}$10]
(h)
α
90°
2.08 Å
1 nm
[110]
[1$\bar{1}$0]
[00$\bar{1}$]

Figure 4

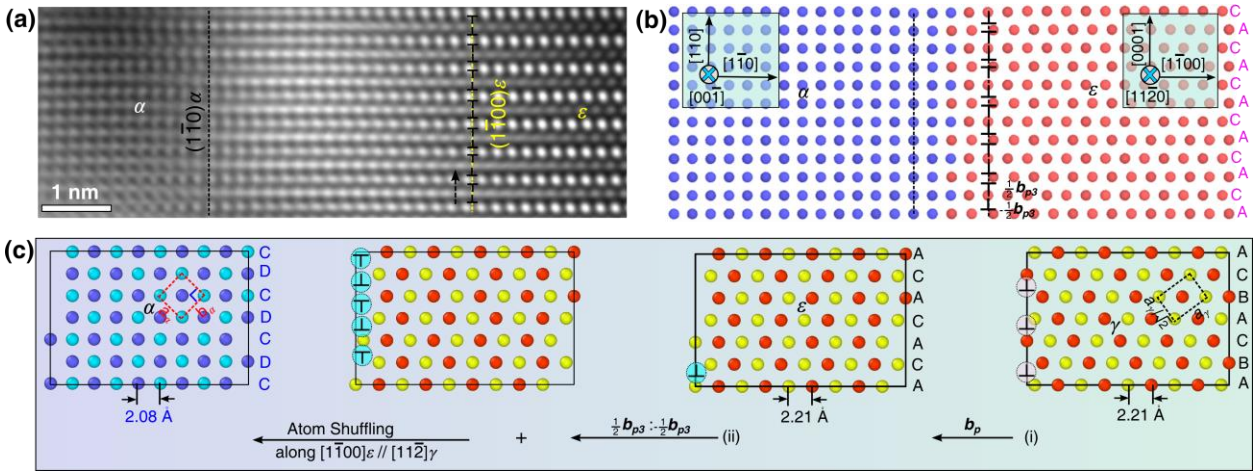
(a)
α
(1$\bar{1}$0)α
(1$\bar{1}$00)ε
ε
1 nm
(b)
[110]
[1$\bar{1}$0]
[00$\bar{1}$]
α
ε
[0001]
[1$\bar{1}$00]
[11$\bar{2}$0]
$\frac{1}{2}b_{p3}$
$\frac{1}{2}b_{p3}$
(c)
2.08 Å
Atom Shuffling
along [1$\bar{1}$00]ε // [11$\bar{2}$]γ
+
$\frac{1}{2}b_{p3}$: $\frac{1}{2}b_{p3}$
(ii)
2.21 Å
b_p
(i)
2.21 Å

Figure 5

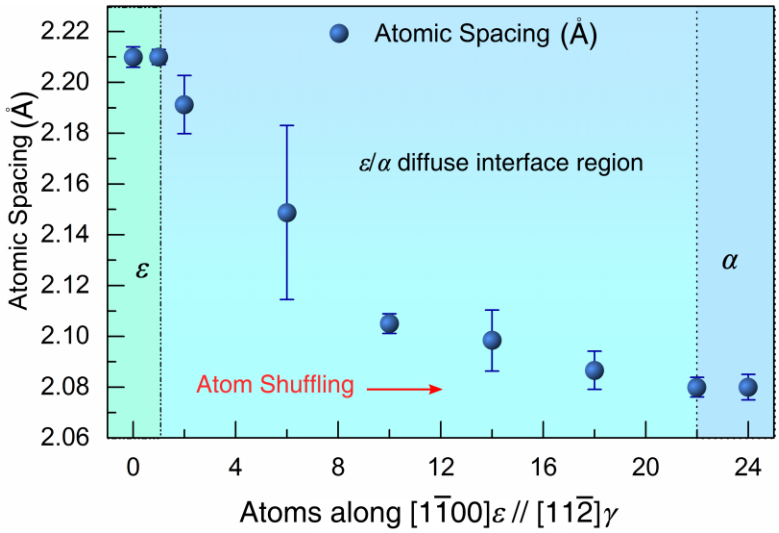
Atomic Spacing (Å)
Atomic Spacing (Å)
2.22
2.20
2.18
2.16
2.14
2.12
2.10
2.08
2.06
ε/α diffuse interface region
ε
α
Atom Shuffling
0
4
8
12
16
20
24
Atoms along [1$\bar{1}$00]ε // [11$\bar{2}$]γ

Figure 6

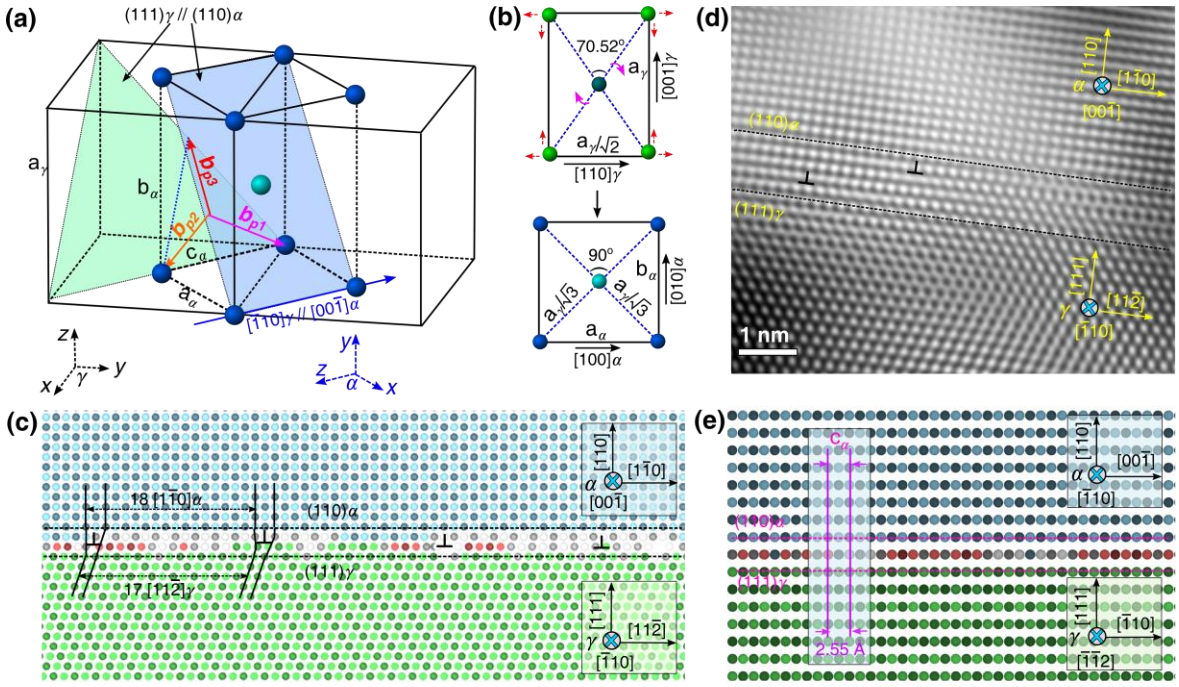
(a)
(111)γ // (110)α
aγ
bα
bp3
bp2
bp1
cα
aα
[1̄10]γ // [00̄1]α
(b)
70.52°
aγ
[001]γ
aγ/√2
[110]γ
90°
bα
[010]α
aγ/√3
aγ/√3
aα
[100]α
(d)
(110)α
(111)γ
1 nm
(c)
18 [1̄1̄0]α
(1̄10)α
17 [11̄2]γ
(111)γ
(e)
cα
(001)α
(111)γ
2.55 Å

Figure 7

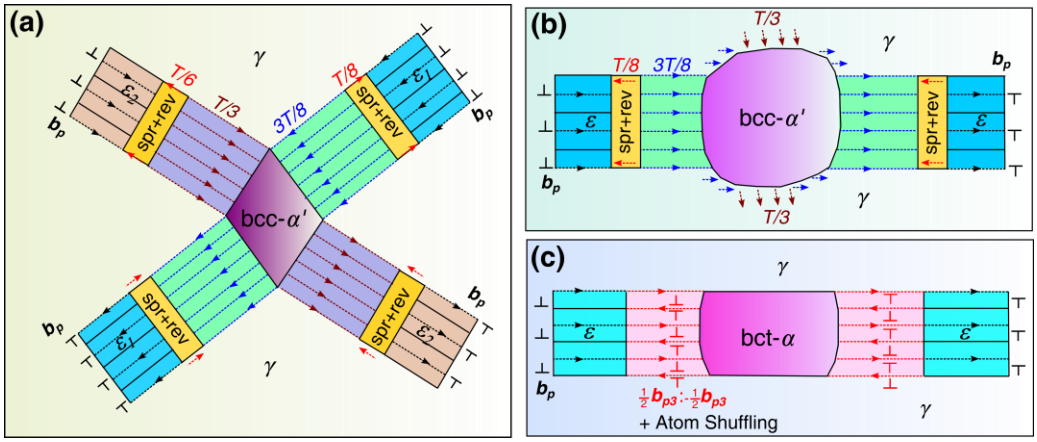
(a)
γ
T/6
T/3
T/8
3T/8
spr+rev
bcc-α′
(b)
T/3
T/8
3T/8
spr+rev
bcc-α′
(c)
bct-α
+ Atom Shuffling

Supplementary Material

Shear and Shuffling Accomplishing Polymorphic fcc γ → hcp ε → bct α Martensitic Phase Transformation

Xu-Sheng Yang[b,1], Sheng Sun[a,1], Hai-Hui Ruan[c], San-Qiang Shi[c,d,**], Tong-Yi Zhang[a,*]

[a]*Shanghai University Materials Genome Institute and Shanghai Materials Genome Institute, Shanghai University, 99 Shangda Road, Shanghai 200444, China*

[b]*Advanced Manufacturing Technology Research Centre, Department of Industrial and Systems Engineering, The Hong Kong Polytechnic University, Hung Hom, Kowloon, Hong Kong, China*

[c]*Department of Mechanical Engineering, The Hong Kong Polytechnic University, Hung Hom, Kowloon, Hong Kong, China*

[d]*Hong Kong Polytechnic University Shenzhen Research Institute, Shenzhen, China*

[1] These authors contributed equally to this work.

[**]. Corresponding author. mmsqshi@polyu.edu.hk (S.-Q Shi). Tel & Fax: +852-27667821

[*]. Corresponding author. mezhangt@ust.hk and zhangty@shu.edu.cn (T.-Y Zhang). Tel & Fax: +86-21-66136172

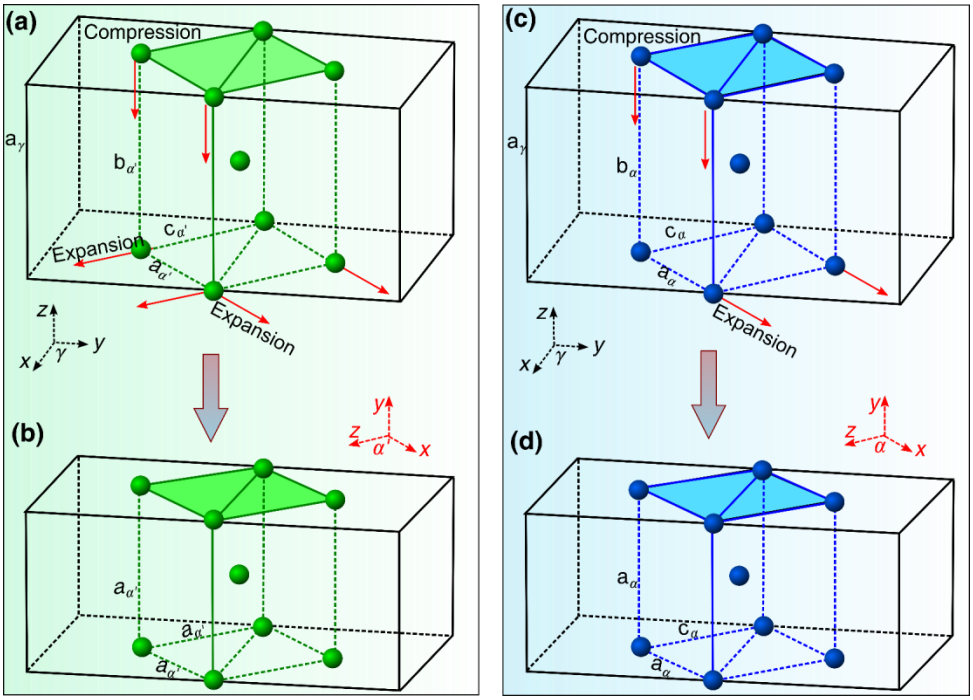

Figure S1 The lattice correspondence for the bcc-α′ (**a, b**) and bct-α (**c, d**). The bcc-α′ with $a_{\alpha'} = b_{\alpha'} = c_{\alpha'}$ can be achieved by a 20% compression of the fcc-γ lattice in the $[001]\gamma$ direction, and an expansion of 12% in both $[110]\gamma$ and $[\bar{1}10]\gamma$ directions. The bct structure with $a_{\alpha} = b_{\alpha} \neq c_{\alpha}$, however, is achieved by a 18.4% compression in the $[001]\gamma$ direction, a 15.3% expansion in the $[110]\gamma$ direction, and maintaining dimension unchanged in the $[\bar{1}10]\gamma$ direction.

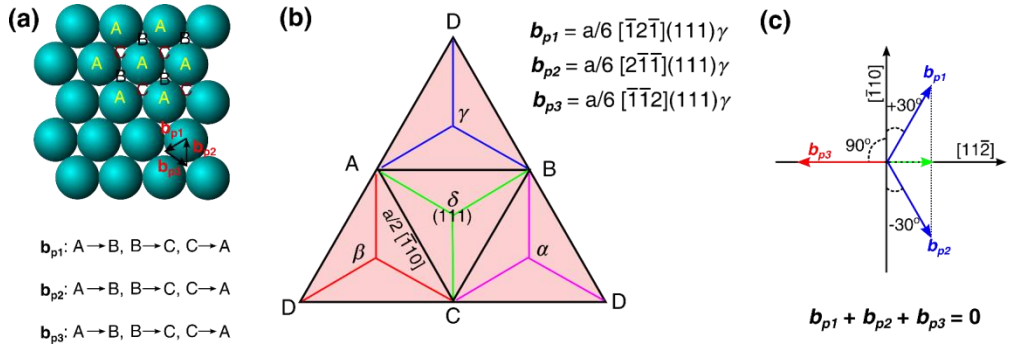

Figure S2. Three types of Shockley partial dislocations on (111)γ plane. Schematic diagrams. (**a**) Three types of Shockley partial dislocations can cause the same stacking fault and change the stacking sequence as: A → B, B → C, C → A. (**b**) Thompson tetrahedron showing three types of Shockley partial dislocations have the Burgers vectors $\boldsymbol{b}_{\mathbf{p1}} = \frac{a_f}{6}[\bar{1}2\bar{1}](111)\gamma$, $\boldsymbol{b}_{\mathbf{p2}} = \frac{a_f}{6}[2\bar{1}\,\bar{1}](111)\gamma$ and $\boldsymbol{b}_{\mathbf{p3}} = \frac{a_f}{6}[\bar{1}\,\bar{1}2](111)\gamma$, respectively. (**c**) Three types of Shockley partial dislocations have different inclined angle with respect to the dislocation lines of $[\bar{1}10]\gamma$.

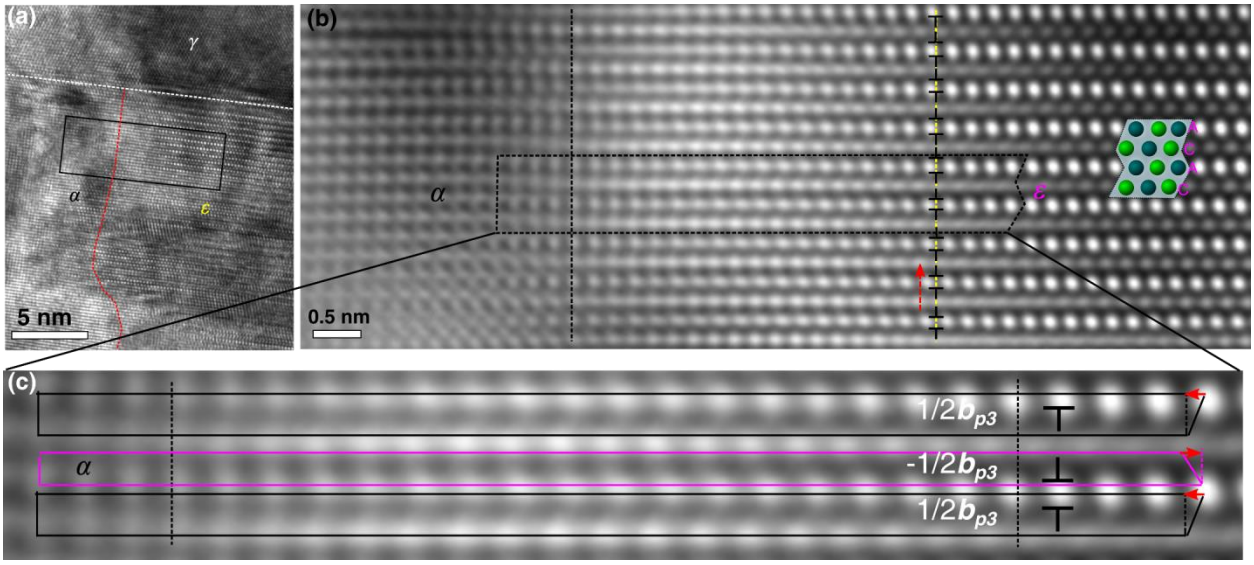

Figure S3. The detailed Burgers circuit for indexing the half Shockley partial dislocation dipoles, $-\frac{1}{2}\boldsymbol{b}_{\mathbf{p3}}:\ \frac{1}{2}\boldsymbol{b}_{\mathbf{p3}}$, in the ε/α interfacial region.

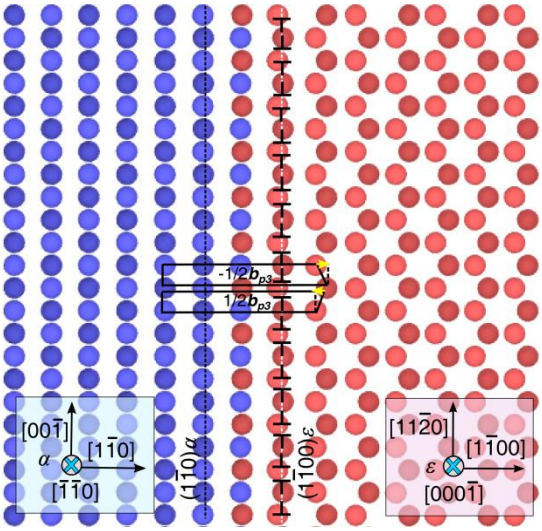

Figure S4. MD simulation image gives the atomic arrangement in the γ/α interfacial region, projected from the $[000\bar{1}]\varepsilon // [\bar{1}\,\bar{1}\,0]\alpha$, showing the array of half Shockley partial dislocation dipoles, $-\frac{1}{2}\boldsymbol{b}_{\mathbf{p3}} : \frac{1}{2}\boldsymbol{b}_{\mathbf{p3}}$.

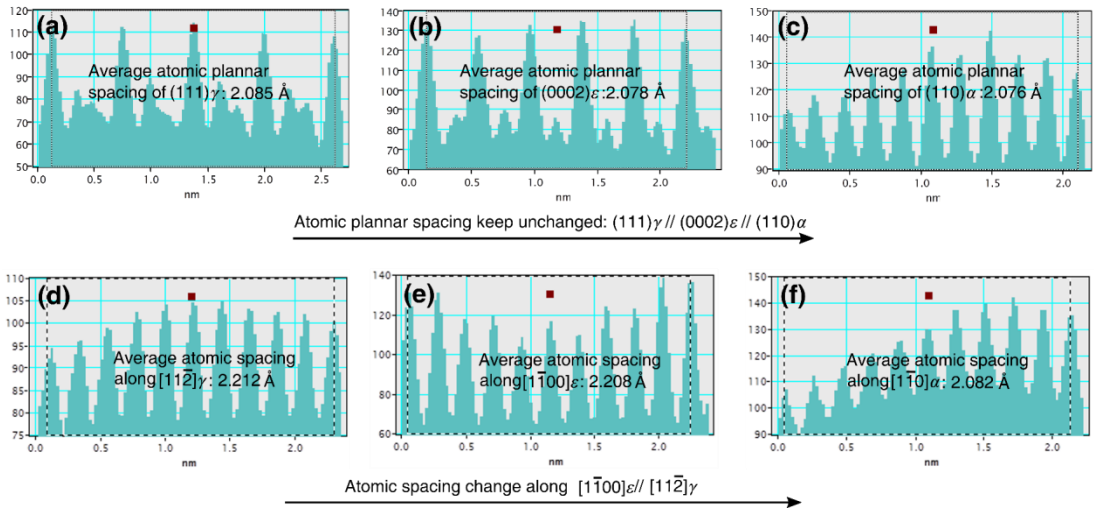

Figure S5. The representative intensity profiles of HRTEM for the atomic plannar spacings of $(111)\gamma$, $(0002)\varepsilon$ and $(110)\alpha$, and the atomic spacings along the $[11\bar{2}]\gamma$, $[1\bar{1}00]\varepsilon$, and $[0\bar{1}1]\alpha$ directions for the parent fcc-γ lattice (**a, d**), hcp-ε lattice (**b, e**), and final bct-α lattice (**c, f**).

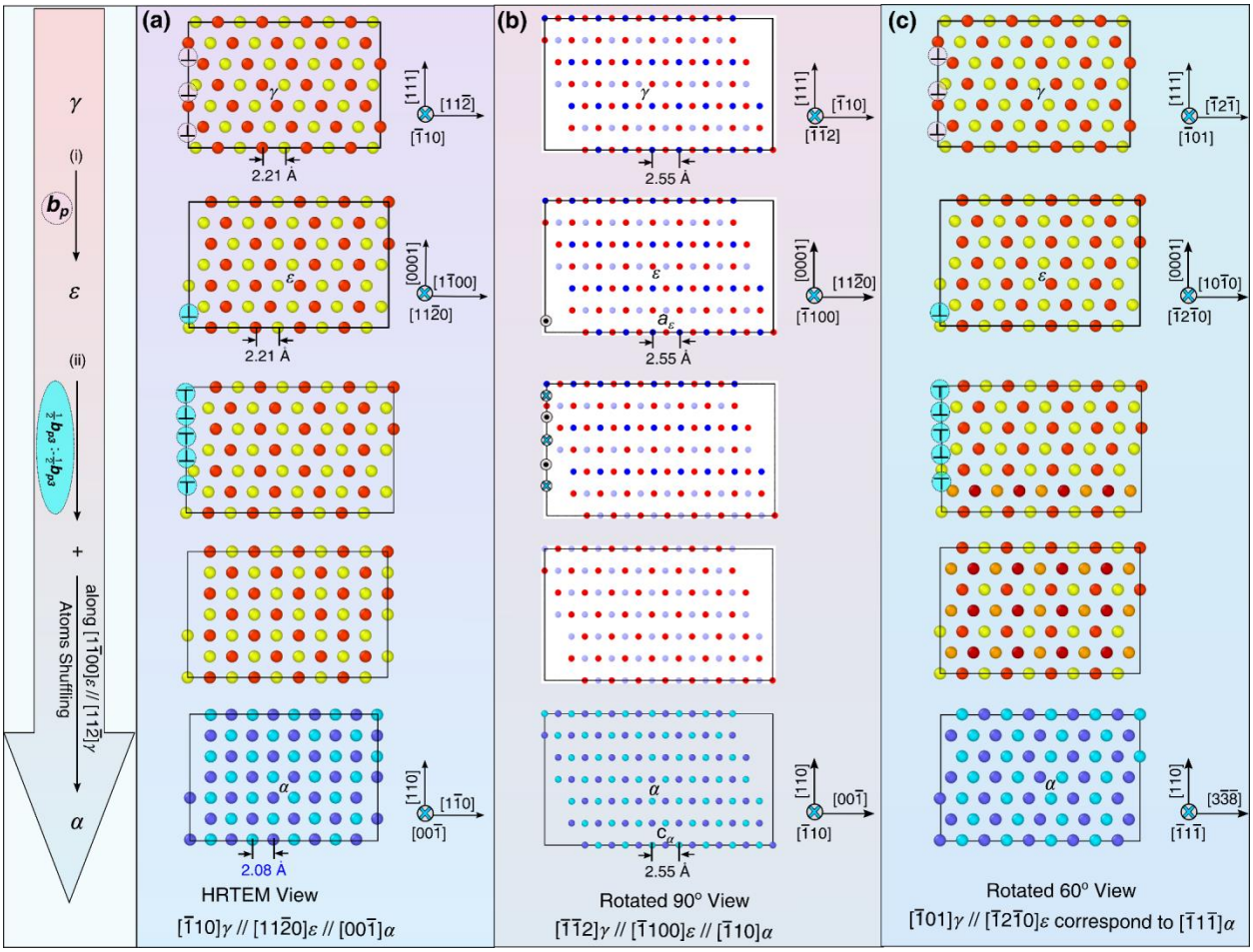

Figure S6. Schematic diagrams for the lattice evolutions from γ, to ε and finally α lattice with different projection view, indicating the role of partial dislocations and atom shuffling along the $[11\bar{2}]\gamma//[1\bar{1}00]\varepsilon$ directions. (**a**) HRTEM view along the $[\bar{1}10]\gamma//[11\bar{2}0]\varepsilon//[00\bar{1}]\alpha$ directions for the lattice evolution. (**b**) Lattice evolution projected along the $[11\bar{2}]\gamma//[1\bar{1}00]\varepsilon//[\bar{1}10]\alpha$ directions (Rotated 90 degrees from the HRTEM view), indicates the value of $c_\alpha = a_\varepsilon = a_\gamma/\sqrt{2}$ = 2.55 Å keeps unchanged in the whole polymorphic MT process. (**c**) Lattice evolution projected along the $[101]\gamma//[\bar{1}2\bar{1}0]\varepsilon$ directions (rotated 60 degrees from the HRTEM view), which correspond to the $[\bar{1}1\bar{1}]\alpha$ direction in the final bct-α lattice.